J Mol Model (2013) 19:5143–5152
DOI 10.1007/s00894-013-2013-7

ORIGINAL PAPER

# Stability and properties of the two-dimensional hexagonal boron nitride monolayer functionalized by hydroxyl (OH) radicals: a theoretical study

**Hong-mei Wang · Yue-jie Liu · Hong-xia Wang · Jing-xiang Zhao · Qing-hai Cai · Xuan-zhang Wang**

Received: 14 July 2013 / Accepted: 12 September 2013 / Published online: 5 October 2013


**Abstract** Motivated by the great advance in graphene hydroxide—a versatile material with various applications—we performed density functional theory (DFT) calculations to study the functionalization of the two-dimensional hexagonal boron nitride (*h*-BN) sheet with hydroxyl (OH) radicals, which has been achieved experimentally recently. Particular attention was paid to searching for the most favorable site(s) for the adsorbed OH radicals on a *h*-BN sheet and addressing the roles of OH radical coverage on the stability and properties of functionalized *h*-BN sheet. The results indicate that, for an individual OH radica, the most stable configuration is that it is adsorbed on the B site of the *h*-BN surface with an adsorption energy of −0.88 eV and a magnetic moment of 1.00 $\mu_B$. Upon adsorption of more than one OH radical on a *h*-BN sheet, however, these adsorbates prefer to adsorb in pairs on the B and its nearest N atoms from both sides of *h*-BN sheet without magnetic moment. An energy diagram of the average adsorption energy of OH radicals on *h*-BN sheet as a function of its coverage indicates that when the OH radical coverage reaches to 60 %, the functionalized *h*-BN sheet is the most stable among all studied configurations. More importantly, this configuration exhibits good thermal and dynamical stability at room temperature. Owing to the introduction of certain impurity levels, the band gap of *h*-BN sheet gradually decreases with increasing OH coverage, thereby enhancing its electrical conductivity.

**Electronic supplementary material** The online version of this article (doi:10.1007/s00894-013-2013-7) contains supplementary material, which is available to authorized users.

H.-m. Wang · Y.-j. Liu · H.-x. Wang · J.-x. Zhao (✉) · Q.-h. Cai · X.-z. Wang
Key Laboratory for Photonic and Electronic Bandgap Materials, Ministry of Education, Harbin Normal University, Harbin 150025, China
e-mail: xjz_hmily@163.com

**Keywords** OH radical · Boron nitride sheet · Adsorption · Density functional theory

## Introduction

Since its discovery in 2004, graphene, a single layer of $sp^2$-bonded carbon atoms tightly packed into a two-dimensional (2D) honeycomb structure, has attracted enormous attention due to its outstanding mechanical, thermal, optical, and electrical properties [1]. These unique properties render graphene a promising material for future technological fields [2–5]. For example, graphene is one of the candidates for next generation electronics because of its high electron mobility [6]. However, the lack of band gap and poor solubility in some solvents has imposed great limitations on its application. Recent studies have shown that chemical functionalization is an effective way to overcome the above drawbacks of graphene. In fact, chemical modification of graphene can not only effectively modify its electronic and magnetic properties, but also greatly enhance its solubility, thus widening its application fields [7, 8]. One of the most important functionalizations of graphene is its attachment to hydroxyl (OH) radical—a hot topic recently [9–18]. This is expected, because graphene functionalized by OH radicals has potential applications in the development of chemical catalysts [12–14], hydrogen storage [15], gas sensors [16], and functional materials [17, 18]. More interestingly, Jiang et al. [10] have reported that the band gap of graphene, which is close to the band gap of Si, can be opened after OH functionalization. This is very important in building graphene-based electronic circuits without the need for cutting or etching.

On the other hand, as a structural analogue of graphene, the 2D hexagon boron nitride (*h*-BN) sheet, which has been

synthesized by various groups [19, 20], exhibits electronic properties distinctly different from graphene due to the large ionicity of its B–N bond. For example, *h*-BN sheet has excellent optical and mechanical properties, high thermal conductivity, and high oxidation and corrosion resistance. Therefore, *h*-BN sheet has wide applications in many fields, such as far ultraviolet light-emitting diodes, field emitters, and polymer-matrix nanocomposites operated in extreme environments [21–25]. However, like its other morphological forms such as nanotubes and nanoribbon, *h*-BN sheet is a semiconductor with a wide band gap (~5.5 eV), which hinders its potential applications for the development of electronic devices to some extent. Recent studies have found that the properties of *h*-BN sheet can be greatly modified through the chemical functionalization [26–40]. Theoretically, various approaches, such as fluorination [26, 27], hydrogenation [26], C [28] or O [29] adatom adsorption, defect introduction [30–34], noncovalent functionalization with organic molecules [35, 36] and charge doping [37], have also been proposed to modulate the properties of *h*-BN sheet. Experimentally, Lin et al. [39] have reported that edge functionalization can be achieved by ultrasonication-assisted hydrolysis of *h*-BN sheets. Sainsbury et al. [40, 41] have demonstrated synthesis of *h*-BN sheet functionalized by oxygen radicals (such as OH radicals), which exhibits significantly enhanced mechanical properties and is a promising candidate for next generation polymer nanocomposites.

In light of experimental studies showing functionalization of *h*-BN sheet with OH radicals and its potential in designing *h*-BN-based devices, it is highly desirable to study the interaction of *h*-BN sheet with OH radicals from a theoretical view point, which can provide helpful insights into the reported experimental results. We should point out that the OH adsorption on *h*-BN sheet was investigated from first principles calculations very recently [38]. Yet, these latter authors consider only the adsorption of two OH radicals on *h*-BN sheet. The following questions are still unanswered: (1) what happens with adsorption of OH radicals at various coverages? (2) How does OH coverage affect the stability of the functionalized *h*-BN sheet? (3) How do the electronic properties of the *h*-BN sheet change due to functionalization of OH radicals at various coverages? To answer the above questions, in this paper, we study the functionalization of *h*-BN sheet with OH radicals at various coverages.

## Computational methods and models

Calculations were based on the spin-polarized DFT using the generalized gradient approximation (GGA) for the exchange-correlation potential prescribed by Perdew-Burke-Ernzerhof (PBE) [42], which was implemented in the DMol$^3$ package [43, 44]. All-electron calculations were employed with the double numerical basis sets plus polarization functional (DNP), which are comparable to the Gaussian 6-31G(d,p) basis set in size and quality. A (5×5) supercell with the periodic boundary conditions on the *x*–*y* plane was employed to model the adsorption of OH radicals at various coverages on the infinite *h*-BN sheet. The vacuum space was set with 20 Å in the *z* direction to avoid interactions between periodic images. A 3×3×1 mesh of *k*-points [45] and a global orbital cutoff of 5.20 Å were used. All structures were fully relaxed without any symmetry constraints. Convergence in energy, force, and displacement were set as $10^{-5}$ Ha, 0.002 Ha/Å, and 0.005 Å, respectively. The Hirshfeld method [46] was adopted to calculate the charge transfer and magnetic moment. The transition state (TS) was determined by calculating the minimum-energy path (MEP) using the nudged elastic band (NEB) method [47, 48].

The average adsorption energy ($E_{ads}$) of OH radical on *h*-BN sheet is defined as: $E_{ads}=(E_{n\,OH/h-BN\ sheet}-E_{h-BN\ sheet}-nE_{OH})/n$, where $n$ is the number of the adsorbed OH radical on *h*-BN sheet. $E_{n\,OH/h\text{-}BN\ sheet}$, $E_{h\text{-}BN\ sheet}$, and $E_{OH}$ are the total energy of the functionalized *h*-BN sheet by $n$ OH radicals, the pristine *h*-BN sheet, and the isolated OH radical, respectively. According to this definition, $E_{ads}$ corresponds to a stable configuration.

## Results and discussion

### Adsorption of a single OH radical on *h*-BN sheet

We first investigated the adsorption of a single OH radical on *h*-BN sheet. As shown in Fig. 1, four different adsorption sites on *h*-BN sheet were considered, including (1) the top of the B ($P_1$) or (2) N ($P_2$) atom, (3) the hollow of the $B_3N_3$ hexagonal ring ($P_3$), and (4) the bridge of the B–N bond ($P_4$). After full geometric optimization of the four initial configurations, it was found that the adsorption of the individual OH radical on top of the B atom was the most energetically favorable, with its H atom pointing in the direction of the center of a 6-fold ring as shown in Fig. 2a. This result is in good agreement with the experimental report [40]. The adsorption energy of this configuration is −0.88 eV, which is slight larger than that of graphene [10, 49]. It is obvious that a covalent bond has formed between OH and the *h*-BN sheet at the B site (Figure S1 in Supporting Information) with a B–O bond length of 1.51 Å. Moreover, OH adsorption induces an apparent radical deformation to the BN sheet, in which the adsorbed B atom by individual OH is pulled outwards from the plane of the sheet by 1.25 Å. Meanwhile, the B–N bond lengths involving OH-adsorbed B atom are 1.53,

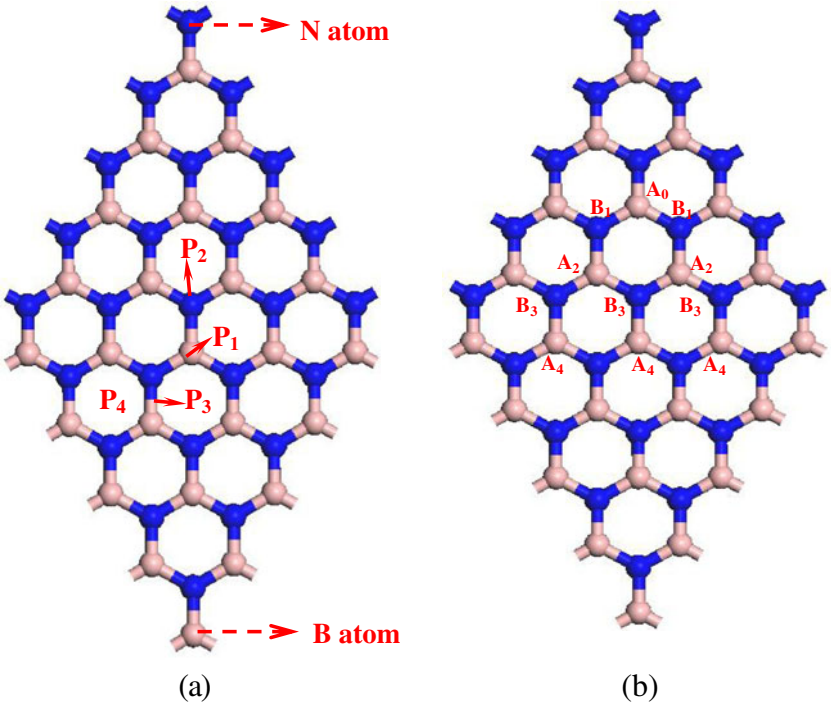


**Fig. 1** Schematic view of various sites of **a** one, **b** two OH radicals adsorbed on the hexagonal boron nitride (*h*-BN) sheet

1.54, and 1.54 Å, respectively, longer than those in the pristine *h*-BN sheet with $sp^2$ hybridization (1.45 Å). Such structural deformation is attributed to the change from $sp^2$ to $sp^3$ hybridization on the adsorbed B atom by OH radical, leading to the destruction of one of the B–N π bonds. In addition, two meta-stable configurations are obtained, where the OH radical is adsorbed on the $P_2$ or $P_3$ site with adsorption energies of −0.36 and −0.35 eV, respectively, as shown in Table 1.

NEB calculations show that the adsorbed OH radical easily diffuses on *h*-BN sheet surface with an energy barrier of 0.56 eV along a path where the O atom in the adsorbed OH radical moves from the top of the B atom to the adjacent B atom (see Fig. 3a), while the H atom remains pointing toward the center of six-fold ring. In the diffusion transition state, OH remains only weakly bound to the *h*-BN sheet, as can be seen from the distance between the OH radical and the *h*-BN sheet, which elongates from 1.51 to about 2.40 Å. Moreover, dissociation of the adsorbed OH radical on BN sheet was found to be highly unfavorable both thermodynamically and kinetically, since the process from the undissociated adsorbed OH radical to the final configuration has an high energy barrier of 1.64 eV and large endothermicity of 1.46 eV as shown in Fig. 3b. This fact indicates that hydrogen atoms prefer to attach to oxygen atoms rather than to *h*-BN sheet in the presence of an oxygen atom, which is similar to the case of graphene [49].

Taking the most stable configuration of the individual OH radical on BN sheet (Fig. 2a) as an example, we demonstrate the effects of its adsorption on the electronic structure of *h*-BN sheet on the basis of the calculated band structure. For comparison, the band structure of the pristine *h*-BN sheet is also calculated (Figure S2). The results indicate that the band gap of the pristine *h*-BN sheet is 4.71 eV, in good agreement with previous reports [26, 35, 50]. However, the adsorption of the individual OH radical gives rise to a flat impurity band above the valance-band edge by 0.11 eV of the band structure of the pristine *h*-BN sheet (Fig. 2b), which is split into spin-up and spin-down branches. The spin-up branch is occupied, while the spin-down branch is empty, leading to a strong spontaneous magnetization of 1 $\mu_B$ in *h*-BN sheet. The spin density (Fig. 2c) suggests that the magnetic moment of this system is attributed mainly to the O atom of the adsorbed OH radical and its three adjacent N atoms. Their contributions to the magnetic moment of the whole system are 20 %, 14 %, 11 %, and 7%, respectively. Moreover, the projected density of states (PDOSs) on the O atom of OH radical, the adsorbed B atom, the neighboring N atoms show that the localized impurity state originates mainly from the O and N atoms (Fig. 2b), which is consistent with the spin density. Because the OH radical lacks one electron, it is understood that this adsorbate would loot electrons from the BN sheet. Hirshfeld analysis shows that the lost electrons (~0.10 *e*) are predominantly from the N atoms around the adsorbed OH radical.

## Adsorption of OH radicals on *h*-BN sheet at various coverages

It is known that the coverage of addends plays an important role on the stability and properties of the functionalized

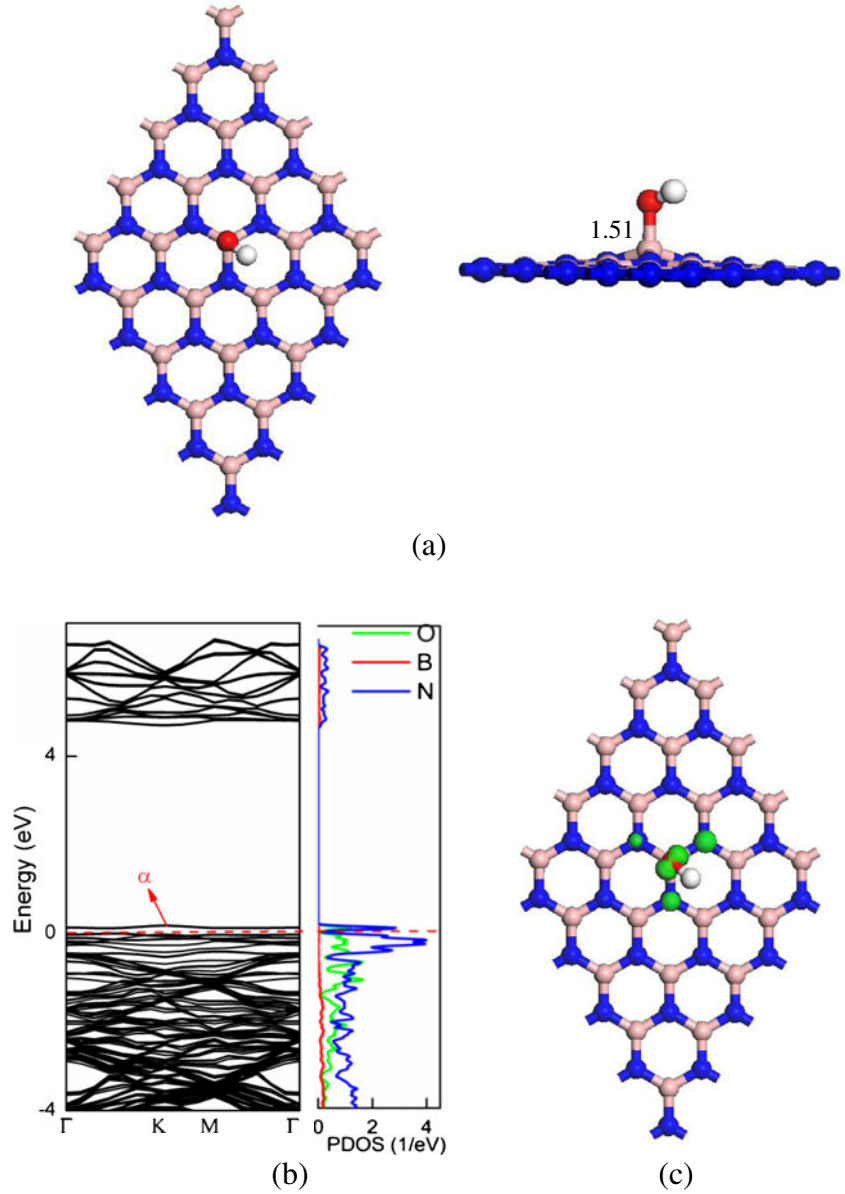


**Fig. 2** **a** Optimized stable configuration. **b** Band structure and projected density of state, where α denoted the induced impurity level. **c** Spin density of an individual OH radical on *h*-BN sheet. The unit of the bond length is Å and the Fermi level is indicated with a *red dotted line*

substrate. Thus, on the basis of the adsorption of one OH radical, we investigated the adsorptions of various numbers ($n$) of OH radicals on *h*-BN sheet, where $n$ equals to 2, 4, 10, 30, and 50, respectively. The corresponding coverage of OH radical is 4 %, 8 %, 20 %, 60 %, and 100 %, respectively. Note that the coverage is defined as the number of OH radicals versus the total number of B and N atoms in the *h*-BN sheet (the adopted supercell in the present work includes 25 B and 25 N atoms).

When two OH radicals are adsorbed on *h*-BN sheet, a number of initial possible configurations were considered as shown in Fig. 1c: the two OH radicals are bound with boron or nitrogen atoms from the same (A–A) or different sublattice (A–B) on one or two sides (A–A′, B–B′, A–B′, and A′–B) of *h*-BN sheet. Moreover, the prime indices are used for the

**Table 1** Parameters for an individual OH radical adsorbed on hexagonal boron nitride (*h*-BN) sheet[a]

| Site | $P_1$ | $P_2$ | $P_3$ |
|---|---|---|---|
| $E_{ads}$ (eV) | −0.88 | −0.36 | −0.35 |
| $d$ (Å)[a] | 1.51 | 2.40 | 2.85 |
| $h$ (Å) | 1.25 | 0.03 | 0.01 |
| μ ($\mu_B$) | 1.00 | 1.00 | 1.00 |
| $Q$ (e) | 0.10 | 0.12 | 0.12 |

[a] $E_{ads}$ is the adsorption energy; $d$ is the shortest distance between adsorbed OH radical and *h*-BN sheet; $h$ denotes the maximum deviation of the adsorbed atom by individual OH radical along the $z$ direction from the *h*-BN sheet plane, μ is the magnetic moment of the whole system, and $Q$ is the charge transfer from *h*-BN sheet to the adsorbed OH radical

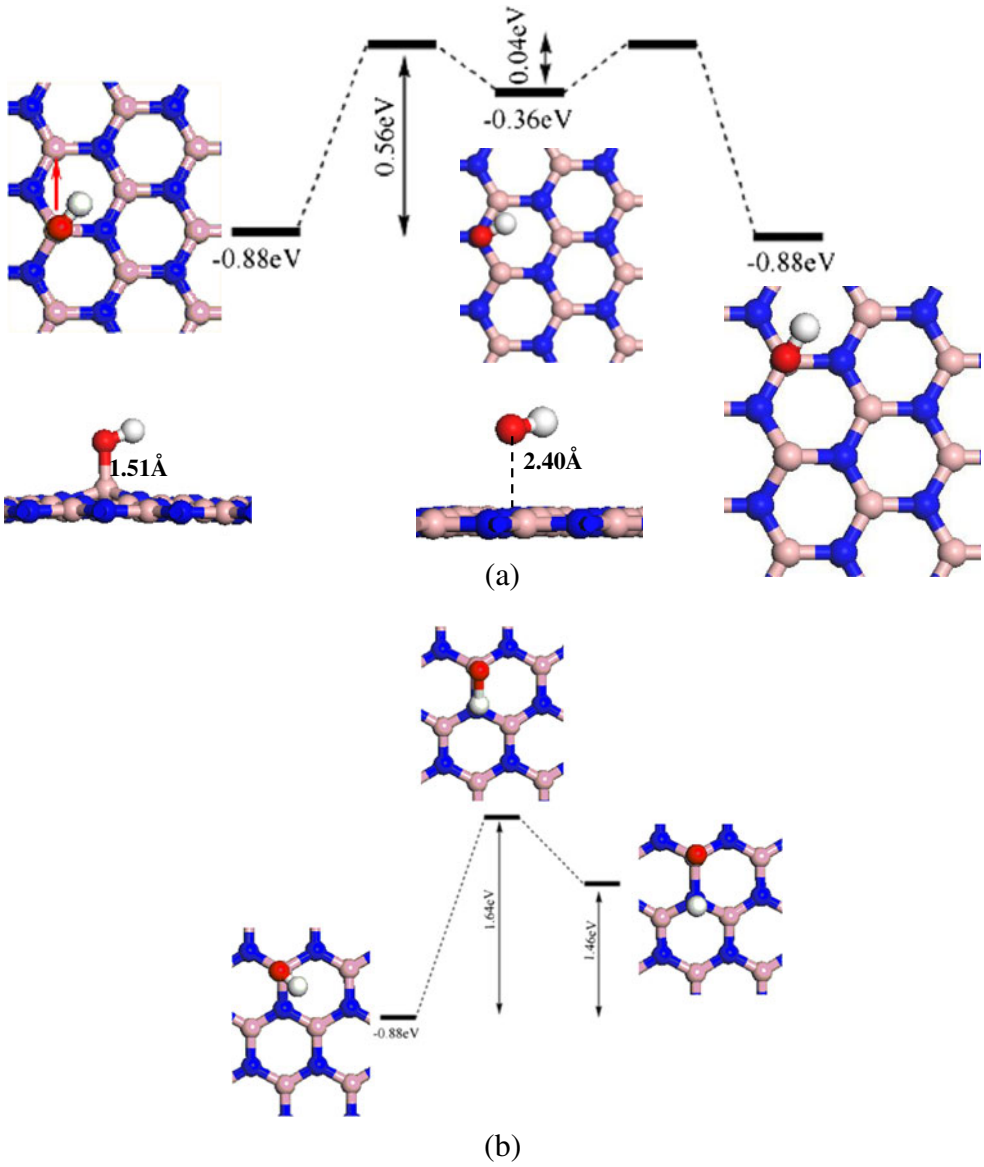


**Fig. 3** **a** The diffusion and (**b**) dissociation process of an individual OH radical adsorbed on *h*-BN sheet

latter. We find that the two adsorbed OH radical on $A_0$–$B_1$, $A_0$–$B_1'$, $A_0$–$B_3$, and $A_0$–$B_3'$ form a nonmagnetic configuration as shown in Table 2. On the contrary, in the case of $A_0$–$A_2$ and $A_0$–$A_2'$, the magnetic moments of the two configurations are basically the same as that of the individual OH radical. Among all configurations listed in Table 2, $A_0$–$B_1'$ is the most stable, where the two OH radicals are located on top of the B atom and its ortho-site N atom on both sides of the *h*-BN sheet. The adsorption energy of this configuration is −1.48 eV per OH radical, which is much larger than that of the most stable configuration of the individual OH radical (−0.88 eV). The 68.2 % increase in the adsorption energy is likely to be

**Table 2** Average adsorption energies ($E_{ads}$), distance between adsorbates and substrates ($d$), magnetic moments (μ) of two OH radicals adsorbed on *h*-BN sheet, and charge transfer from *h*-BN sheet to OH radicals ($Q$)

| Configuration | $A_0-B_1$ | $A_0-B_1'$ | $A_0-A_2$ | $A_0-A_2'$ | $A_0-B_3$ | $A_0-B_3'$ | $A_0-A_4$ | $A_0-A_4'$ |
|---|---|---|---|---|---|---|---|---|
| $E_{ads}$ (eV) | −1.23 | −1.48 | −0.70 | −0.65 | −0.83 | −0.15 | −0.36 | −0.39 |
| $d$ (Å)[a] | 1.50 | 1.46 | 1.50 | 1.51 | 1.51 | 1.48 | 1.51 | 1.50 |
| μ($\mu_B$) | 0.00 | 0.00 | 1.00 | 1.00 | 0.00 | 0.00 | 1.00 | 1.00 |
| $Q$(e) | 0.07 | 0.08 | 0.10 | 0.09 | 0.08 | 0.08 | 0.10 | 0.10 |

[a] $d$ refers to the shortest distance between the adsorbed OH radical and the plane of *h*-BN sheet

due to a smaller tension being incurred for dual-site chemisorption. Furthermore, the newly formed B–O and N–O bond lengths are 1.46 and 1.49 Å. Because the OH-adsorbed B and N atoms change from $sp^2$ to $sp^3$ hybridization, obvious structural deformations in the *h*-BN sheet can be observed upon adsorption of two OH radicals: (1) the adsorbed B and N atoms are displaced out of the plane of the *h*-BN sheet; (2) the B–N bond length between the two OH radicals is elongated from 1.45 Å (pristine *h*-BN sheet) to the present 1.64 Å.

To find the most stable configuration of a second OH radical on *h*-BN sheet in which a first is located, we also estimated the energy barrier of its diffusion from the top of one N atom to its nearest N atom (Fig. 4). In the diffusion transition state, the shortest distance between the second OH radical and BN sheet is about 1.94 Å. The barrier of diffusion of the seconded OH radical on the N atom is as high as 1.71 eV. Meanwhile, this process is endothermic by 1.33 eV. Hence, we expect that the diffusion of the second OH radical cannot occur at room temperature. This can be understood from the following explanation: the chemisorption of one OH group on one of the B atoms makes the free radical transfer from the OH group to the adjacent N atoms of the B atom involving OH adsorption, leading to the "activation" of these N atoms. As a result, the addition of the second OH radical to the "activated" N atoms is very desirable. In other words, OH radicals prefer to adsorb onto *h*-BN sheet in pairs.

Although a single OH radical can induce magnetic properties in *h*-BN sheet, the two adsorbed OH radicals at the ortho position on both sides of *h*-BN sheet form a nonmagnetic configuration. The average charge transfer from *h*-BN sheet to OH radicals is about 0.08 *e*. The band structure and PDOS of the most stable configuration for two OH radicals on *h*-BN sheet are displayed in Fig. 5. It is shown that the band gap is reduced to 3.46 eV due to the introduction of an empty impurity state within the band gap

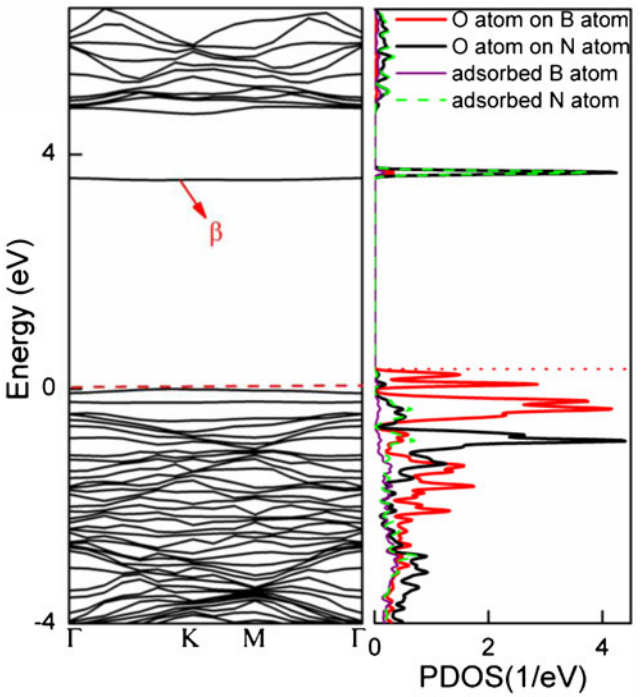


**Fig. 5** Calculated band structure and projected density of state of a pair of OH radicals on *h*-BN sheet, where β denotes the induced impurity level. The Fermi level is plotted with the *red dotted line*

of *h*-BN sheet, which lies deeply below the valence band edge (VBE). The PDOS analysis indicates that the impurity states within the band gap are contributed mainly by the O atom of the adsorbed OH radical on the B atom.

Since OH radicals can form an ordered phase on graphene, can they form a similar configuration on *h*-BN sheet or not? If so, what is the OH coverage for the most stable configuration? To answer the above questions, we investigated the adsorption of OH radicals at several coverages on *h*-BN sheet, i.e., 8 % (4 OH radicals), 20 % (10

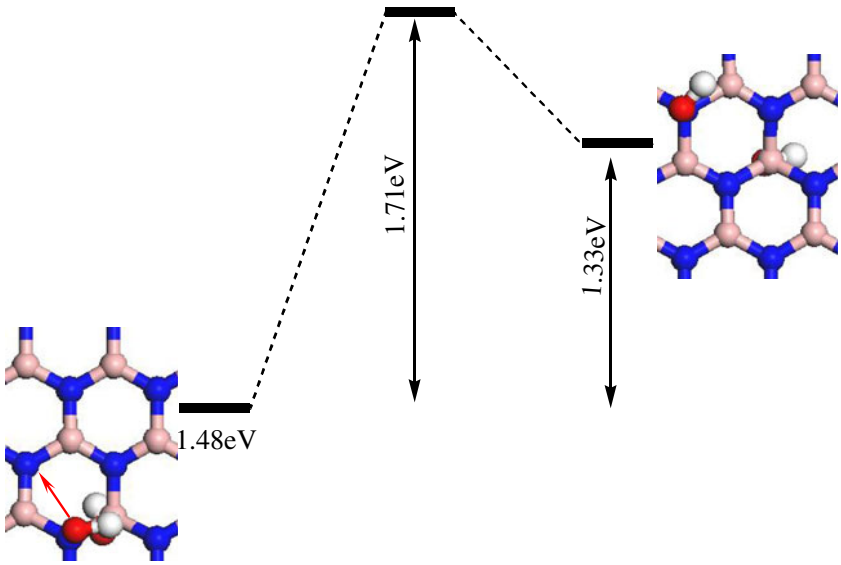


**Fig. 4** Diffusion process of a second OH radical on *h*-BN sheet where the first OH radical is located on the B site

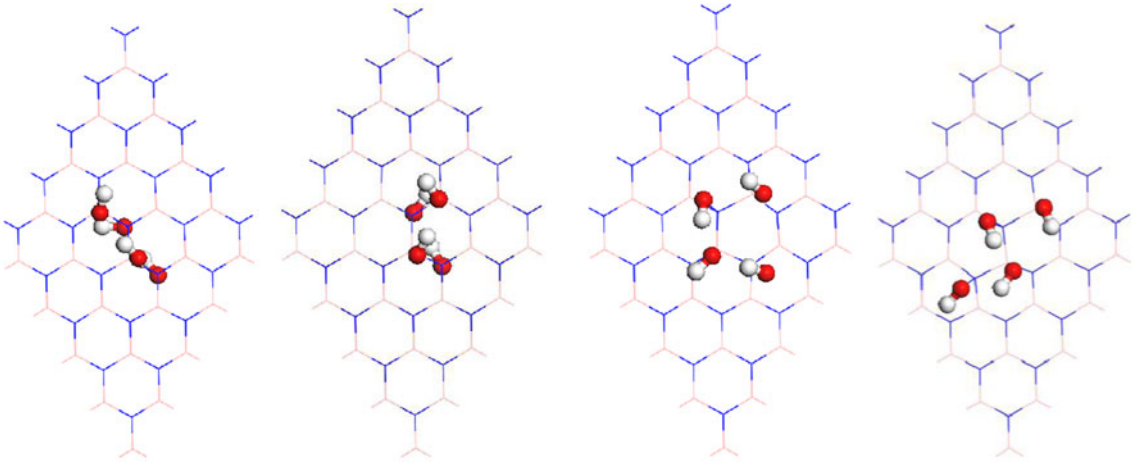

(a) $E_{ads}$ = -1.68 eV (b) $E_{ads}$ = -1.48 eV (c) $E_{ads}$ = -0.54 eV (d) $E_{ads}$ = -0.25 eV

**Fig. 6** The obtained stable configuration and respective adsorption energies of 8 % OH coverage on *h*-BN sheet

OH radicals), 60 % (30 OH radicals), and 100 % (50 OH radicals). In the case of four OH radicals, they can be attached to the *h*-BN sheet from the same side or both sides along a line in zigzag or armchair configurations, forming a very stable aggregate. As shown in Fig. 6, we find that the linear adsorption structures along a zigzag chain on both sides of the *h*-BN sheet are the most favorable. The average adsorption energy of this configuration is −1.68 eV, slightly larger (by 0.20 eV) than that of armchair chains on both sides. Considering that the two configurations in Fig. 6a and b have enough space and less steric repulsion for the adsorbed OH radicals than those of Fig. 6c and d, it is not surprising that the former are more stable the latter. In addition, we note that one OH radical is slanted towards the O atom of the other OH radical, leading to the formation of hydrogen bonds between two OH radicals. For example, in the most stable adsorption configuration (Fig. 6a), the lengths of the O-H…O bonds are about 1.86 (the two OH radicals locate on B atoms) and 1.74 Å (the two OH radicals locate on N atoms).

In the most stable configuration of 20 % OH coverage shown in Fig. 7a, ten OH radicals are attached to *h*-BN sheet in a symmetric style, where these OH radicals are adsorbed in pairs on the both sides of sheet. Among the ten adsorbed molecules, five OH radicals locate on the B sites of the same side of *h*-BN sheet with an average B-O distance of 1.45 Å, while the other five are chemisorbed on the N atoms on the other side of *h*-BN sheet with the average N-O distance of 1.48 Å. Similar to the case of 8 % OH coverage, certain amount of hydrogen bonds forms between these adsorbed OH radicals.

**Fig. 7** The obtained stable configuration and the respective adsorption energies of (**a**) 20 %, (**b**) 60 %, and (**c**) 100 % OH coverage on *h*-BN sheet

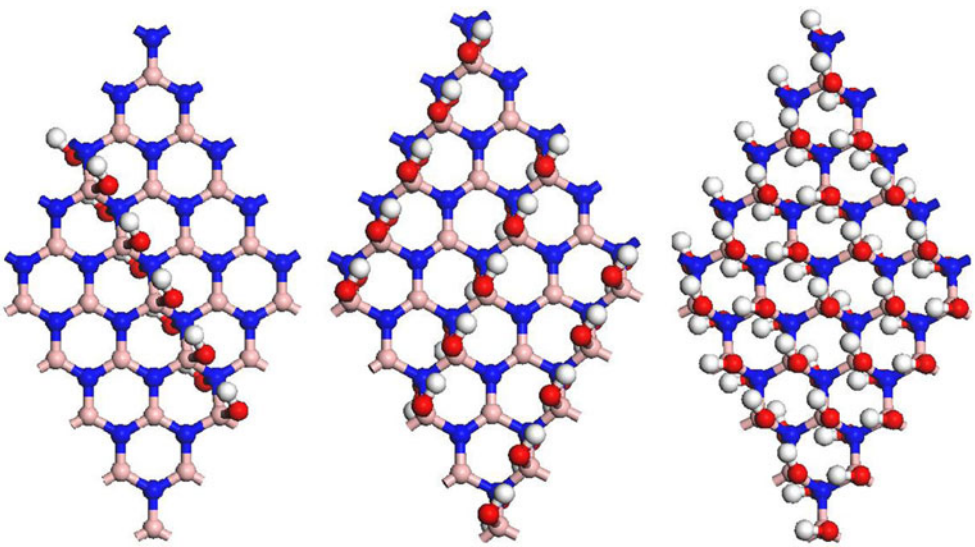

(a) $E_{ads}$ = -1.84 eV (b) $E_{ads}$ = -1.91 eV (c) $E_{ads}$ = -1.78 eV

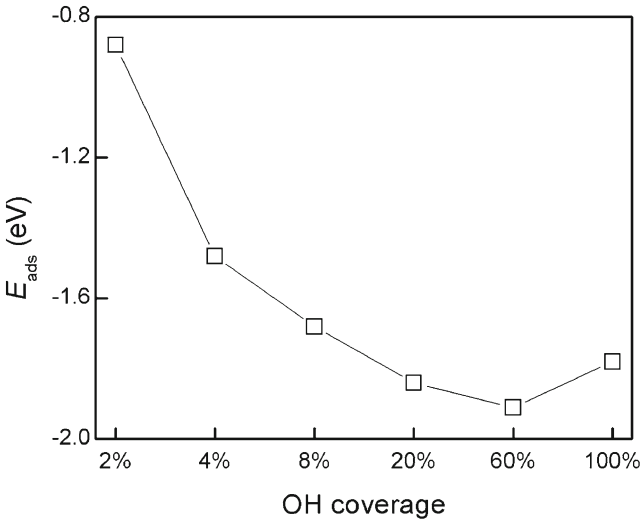


**Fig. 8** Variation in adsorption energies (per OH radical) as a function of OH coverage for their corresponding most stable configurations

The adsorption energy is −1.84 eV per OH radical for this configuration. Figure 7b displays the most stable configuration of 60 % OH coverage, in which the adsorbed OH radicals are located on B and N atoms in pairs with the average lengths of B-O and N-O bonds of 1.43 and 1.48 Å, respectively. The adsorption energy of this configuration is −1.91 eV per OH radical. In the case of 100 % OH coverage, all B and N atoms are covered by 50 OH radicals as listed in Fig. 7c, whose adsorption energy per OH radical is −1.78 eV and the average B-O and N-O bond lengths are 1.41 and 1.48 Å, respectively.

In Fig. 8, the adsorption energy per OH radical is presented as a function of OH coverage. In general, the adsorption energy per OH radical increases, apparently with the increase in OH coverage at low coverage (< 60 %). At high coverage, however, OH radicals repulse each other due to the formation of more hydrogen bonds. As a result, full coverage (100 %) is not the most stable configuration, similar to the case of graphene [10]. Interestingly, the linear adsorption structures along zigzag chains at the OH coverage of 60 % is shown to be the most stable structure among all considered configurations in the present work, in which the B–N bonds are covered by OH radical alternatively.

Another important issue is the stability of the functionalized *h*-BN sheet with OH radicals at room temperature because most electronics work at room temperature. To make sure that this functionalized *h*-BN sheet will be useful for future electronics, first-principle molecular dynamics simulations in NVT (constant number of particles volume temperature) ensemble at room temperature (T= 300 K) with a time step of 1 fs were carried out; *h*-BN sheet functionalized at an OH coverage of 60 % is taken as an example. The fluctuation of energy and temperature with time during the simulation is plotted in Fig. 9. We find that the geometry is still intact after running 3,000 steps, suggesting that this nanomaterial exhibits good thermal stability at room temperature. Moreover, no imaginary frequency was found, and the lowest frequency is about 47.0 $cm^{-1}$, suggesting that this structure is dynamically stable.

Finally, we explore the effects of functionalization of OH radicals at various coverages on the electronic properties of *h*-BN sheet. Because some impurity levels are introduced within the band gap of the BN sheet, this band gap is obviously decreased from 4.71 to 3.41 (by about 27 % change), 3.30 (by about 30 % change), 3.25 (by about 31 % change), and 2.72 eV (by about 42 % change),

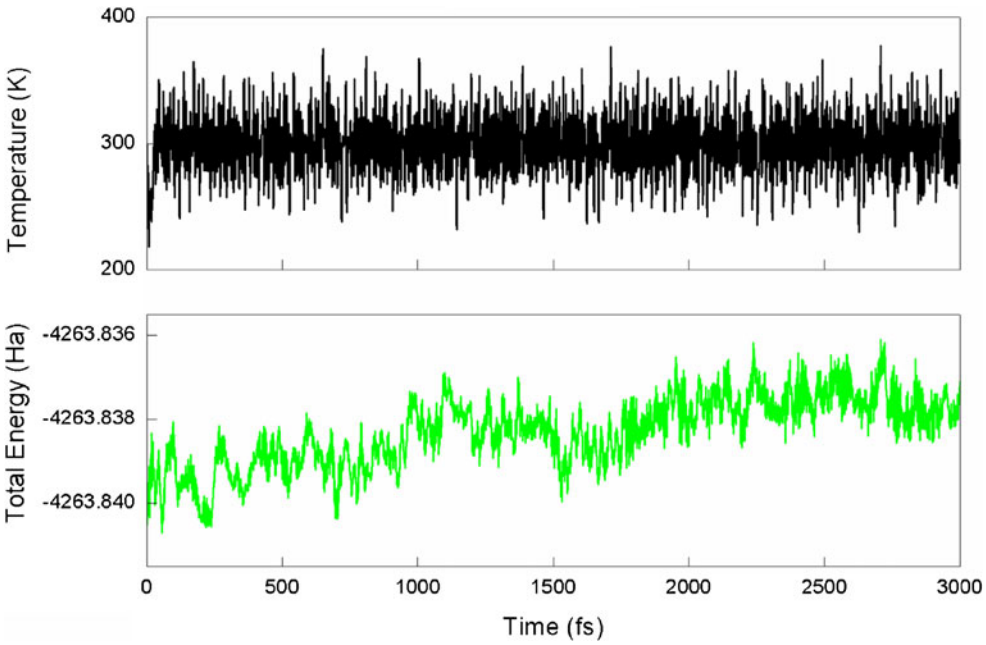


**Fig. 9** Changes in temperature and energy of the most stable functionalized *h*-BN sheet by OH radicals with times obtained from first-principle molecular dynamics simulation

respectively, at OH coverages of 8 %, 20 %, 60 %, and 100 %. This decrease in band gap would result in an electrical conductivity change of the *h*-BN sheet according to the following equation: $\sigma \propto \exp\left(\frac{-E_g}{2kT}\right)$ , where $\sigma$ is the electric conductivity and $k$ is the Boltzmann constant [51]. According to the equation, smaller values of $E_g$ at a given temperature lead to larger electric conductivity. Therefore, the predicted substantial decrement of $E_g$ in *h*-BN sheet upon the adsorption of OH radicals at various coverages enhances its electric conductivity to different degrees, although the functionalized BN sheets are still semiconductors with wide band gaps. In other words, the functionalization of *h*-BN sheet with OH radicals not only enhances its solubility, but also effectively modifies its electronic properties, which will be useful in the development of *h*-BN sheet-based electronics. Although current DMol3 based DFT-GGA calculations are not very accurate in terms of the absolute magnitude of the band gap, we expect that our qualitative results on the effects of OH functionalization on the electronic properties of *h*-BN sheet remain robust with more accurate calculations.

## Conclusions

By carrying out systematic density functional theory calculations, we have studied the functionalization of the pristine *h*-BN sheet with OH radicals at various coverages. The results show that, when a single OH radical is attached to *h*-BN sheet, it prefers to chemisorb on the top of B atom of *h*-BN sheet with an adsorption energy of −0.88 eV. Moreover, the adsorbed individual OH radical can diffuse with an energy barrier of 0.56 eV, while it would not dissociate due to the high barrier (1.64 eV) and large endothermicity (1.46 eV). Upon adsorption of more OH radicals on *h*-BN sheet, it is found that these adsorbates are preferable to adsorb on both sides of *h*-BN sheet in pairs without magnetic moment. Among all studied configurations, the most stable functionalized *h*-BN sheet is that the substrate is covered by 30 OH radicals (60 % coverage), which is shown to possess good stability at room temperature both thermally and dynamically. Because certain impurity states are introduced, the band gap of *h*-BN sheet is greatly reduced after OH adsorption, thereby enhancing the electric conductivity of the *h*-BN sheet. Our results may be useful not only to deeply understand the experimental results, but also to further fabricate *h*-BN sheet-based nanodevices.

**Acknowledgments** This work is supported by the National Nature Science Foundation of China (No. 21203048), the National Nature Science Foundation of Heilongjiang Province (No. B201011), Scientific Research Fund of Heilongjiang Provincial Education Department (NO: 12531195), and the University Key Teacher Foundation of Heilongjiang Provincial Education Department (No. 1252G030).

## References

1. Novoselov KS, Geim AK, Morozov SV, Jiang D, Zhang Y, Dubonos SV, Grigorieva IV, Firsov AA (2004) Science 306:666–669
2. Terronesa M, Botello-Méndez AR, Campos-Delgado J, López-Urías F, Vega-Cantú YI, Rodríguez-Macías FJ, Elías AL, Muñoz-Sandoval E, Cano-Márquez AG, Charlier J-C, Terrones H (2010) Nanotoday 5:351–372
3. Biró LP, Nemes-Incze P, Lambin P (2012) Nanoscale 4:1824–1839
4. Allen MJ, Tung VC, Kaner RB (2010) Chem Rev 110:132–145
5. Dai LM (2013) Acc Chem Res 46:31–42
6. Schwierz F (2010) Nat Nanotechnol 5:487–496
7. Georgakilas V, Otyepka M, Bourlinos AB, Chandra V, Kim N, Kemp KC, Hobza P, Zboril R, Kim KS (2012) Chem Rev 112:6156–6214
8. Kuila T, Bose S, Mishra AK, Khanra P, Kim NH, Lee JH (2012) Prog Mater Sci 57:1061–1105
9. Chen D, Feng HB, Li JH (2012) Chem Rev 112:6027–6053
10. Zhu Q, Liu YH, Jiang JZ (2011) J Phys Chem Lett 2:1310–1314
11. Zhu Y, Murali S, Cai W, Li X, Suk JW, Potts JR, Ruoff RS (2010) Adv Mater 22:3906–3924
12. Pyun J (2011) Angew Chem Int Ed 50:46–48
13. Yang M, Zhou M, Zhang A, Zhang C (2012) J Phys Chem C 116: 22336–22340
14. Li F, Zhao JJ, Chen ZF (2012) J Phys Chem C 116:2507–2514
15. Wang L, Lee K, Sun YY, Lucking M, Chen ZF, Zhao JJ, Zhang SB (2009) ACS NANO 3:2995–3000
16. Tang SB, Cao ZX (2011) J Chem Phys 134:044710–044723
17. Dikin DA, Stankovich S, Zimney EJ, Piner RD, Dommett GHB, Evmenenko G, Nguyen ST, Ruoff RS (2007) Nature (London) 448:457–460
18. Burress JW, Gadipelli S, Ford J, Simmons JM, Zhou W, Yildirim T (2010) Angew Chem Int Ed 49:8902–8904
19. Golberg D, Bando Y, Huang Y, Terao T, Mitome M, Tang C, Zhi C (2010) ACS Nano 4:2979–2993
20. Lin Y, Connell JW (2012) Nanoscale 4:6908–6939
21. Kubota Y, Watanabe K, Tsuda O, Taniguchi T (2007) Science 317:932–934
22. Chen ZG, Zou J (2011) J Mater Chem 21:119
23. Zhi C, Bando Y, Tang C, Kuwahara H, Golberg D (2009) Adv Mater 21:2889–2893
24. Wang Y, Shi Z, Yin J (2011) J Mater Chem 21:11371–11377
25. Yu J, Huang X, Wu C, Wu X, Wang G, Jiang P (2012) Polymer 53:471–480
26. Zhou J, Wang Q, Sun Q, Jena P (2010) Phys Rev B 81:085442
27. Wang Y, Ding Y, Ni J (2010) Phys Rev B 81:19340–19343
28. Li J, Zhou G, Chen Y, Gu BL, Duan W (2009) J Am Chem Soc 131:1796–1801
29. Zhao Y, Wu XJ, Yang JL, Zeng XC (2012) Phys Chem Chem Phys 14:5545–5550
30. Si MS, Xue DS (2007) Phys Rev B 75:193409–193412
31. Si MS, Li JY, Shi HG, Niu XN, Xue DS (2009) Eur Phys Lett 86: 46002–46007
32. Azevedo S, Kaschny JR, de Castilho CM, de B Mota F (2007) Nanotechnology 18, 495707
33. Chen W, Li Y, Yu G, Zhou Z, Chen Z (2009) J Chem Theory Comput 5:3088–3095
34. Kan M, Zhou J, Wang Q, Sun Q, Jena P (2011) Phys Rev B 84: 205412–205416
35. Tang Q, Zhou Z, Chen Z (2011) J Phys Chem C 115:18531–18537
36. Lin Q, Zou X, Zhou G, Liu R, Wu J, Li J, Duan W (2011) Phys Chem Chem Phys 13:12225–12230
37. Zhang Z, Guo W (2011) J Phys Chem Lett 2:2168–2173
38. Bhattacharya A, Bhattacharya S, Das GP (2012) Phys Rev B 85: 035415–035424

39. Lin Y, Williams TV, Xu TB, Cao W, Elsayed-Ali HE, Connell JW (2011) J Phys Chem C 115:2679–2685
40. Sainsbury T, Satti A, May P, Wang Z, McGovern I, Gun'ko YK, Coleman J (2012) J Am Soc Chem 134:18758–18771
41. Sainsbury T, Satti A, May P, O'Neill A, Nicolosi V, Gun'ko YK, Coleman JN (2012) Chem Eur J 18:10808–10812
42. Perdew JP, Burke K, Ernzerhof M (1996) Phys Rev Lett 77:3865–3868
43. Delley B (1990) J Chem Phys 92:508–517
44. Delley B (2000) J Chem Phys 113:7756–7764
45. Monkhorst HJ, Pack JD (1976) Phys Rev B 13:5188–5192
46. Hirshfeld FL (1977) Theor Chim Acta 44:129–138
47. Henkelman G, Jo' sson H (2000) J Chem Phys 113:9978–9985
48. Olsen RA, Kroes GJ, Henkelman G, Arnaldsson A, Jo' sson H (2004) J Chem Phys 121:9776–9792
49. Ghaderi N, Peressi M (2010) J Phys Chem C 114:21625–21630
50. Topsakal M, Akturk E, Ciraci S (2009) Phys Rev B 79:115442–115452
51. Li S (2006) Semiconductor physical electronics, 2nd edn. Springer, New York